ELSEVIER

Journal of Organometallic Chemistry 656 (2002) 156–167

Journal of Organometallic Chemistry

www.elsevier.com/locate/jorganchem

Carbon chain bridged metals: a theoretical approach. Odd chains

Paola Belanzoni [a,*], Nazzareno Re [b], Antonio Sgamellotti [a]

[a] *Dipartimento di Chimica e Istituto CNR di Scienze e Tecnologie Molecolari, Università di Perugia, via Elce di Sotto 8, I-06123 Perugia, Italy*
[b] *Facoltà di Farmacia, Università G. D'Annunzio, I-66100 Chieti, Italy*

Received 11 February 2002; accepted 16 May 2002

Abstract

A theoretical investigation (DFT) allowed us to single out the most appropriate valence structure for the [M–C_x–M′] unit in a variety of homonuclear [{$Cp(CO)_2M$}$_2$(μ-C_x)] (M = Cr, Fe^+, $x = 3$; M = Mn, $x = 3, 5, 7$) and heteronuclear [{$Cp(CO)_2M$}(μ-C_x){$Cp(CO)_2M'$}] (M = Fe^+, M′ = Mn, $x = 3$; M = Fe, M′ = Cr, $x = 3, 5, 7$) model compounds and to foresee it on the basis of the molecular parameters, such as (i) the nature of the metals and their oxidation states; (ii) the d^n configurations and the metal coordination numbers; (iii) the chain length. The valence structure of the [M–C_x–M′] unit is diagnostic of the metal-to-metal communication. A simple electron-counting scheme has been developed to predict the valence structure, based on the d^n configuration of the ML_m ($M'L'_{m'}$) fragments and the number of p_π electrons of the 'linear' C_x unit. © 2002 Elsevier Science B.V. All rights reserved.

Keywords: Carbon chain bridged metals; Odd carbon bridges; Density functional calculations; Cumulenic versus polyynyl/carbyne valence structure

1. Introduction

Several organometallic complexes in which two transition metal atoms are bridged by linear unsatured carbon chains, $L_mMC_xML_m$, have recently attracted much interest [1–4]. Indeed, they constitute a first step in the synthesis of elemental carbon forms stabilized by transition metal complexes. In particular, μ-C_x bridged dinuclear complexes are now available for $x = 2$–20 [5] and constitute one of the most interesting examples of one-dimensional molecular wires. On increasing the length of the C_x chain, analogies with poly-acetilene and the possibility of long range interactions between the two metals become apparent.

All the synthesized μ-C_x bridged complexes present a number of common features: (i) the metal fragments spanning the bridge are constituted by mid to late transition metals in low oxidation state with π-acceptor ligands (ii) particularly widespread are fragments like CpMLL′ (L,L′ = CO, NO, PR_3; M = Mn, Re, Fe, Ru) with a coordination number five (iii) the metal configurations of these fragments are mainly d^5, d^6 and d^7 with very few lower electron counts.

Among the several μ-C_x bridged dinuclear complexes which have been synthesized, structural and synthetic reasons suggest to distinguish between compounds with an even number of carbon atoms (C_{2x}) and those with an odd number of carbon atoms (C_{2x+1}). This difference is already evident in the simple HC_xH series (known only for even x) [6] and arises from the different nature of the ground states for compounds with an even and an odd number of carbon atoms; a stable closed shell singlet in the former case and an unstable open shell triplet in the latter case [7]. Bridged dinuclear compounds with an even C_x bridge are by far more common. Several four-carbon bridged complexes are known with structures similar to those of butadiyne, described as alternating single and triple bonds [8–19], such as [{Cp*Re(PPh_3)(NO)}$_2$(μ-C_4)] [8,9] and [{Cp*Fe(dppe)}$_2$(μ-C_4)] [18,19]. A few C_6 and C_8 bridged complexes, such as [{Cp*Re(PPh_3)(NO)}$_2$(μ-C_6)] and [{Cp*Re(PPh_3)(NO)}$_2$(μ-C_8)] [20], or [{Cp*Fe(dppe)}$_2$(μ-C_8)] [21], have also been synthesized and show an analogous polyynic structure. Recently, [{Cp*Re(PPh_3)}(NO)}$_2$(μ-C_x)] ($x = 6$–20) and [{(C_6F_5)(p-tol_3P)$_2$Pt}$_2$(μ-C_x)] ($x = 8$–16) compounds containing longer even-carbon chains ($x = 12$–20) have

* Corresponding author. Fax: +39-075-585-5606
E-mail address: paola@thch.unipg.it (P. Belanzoni).

0022-328X/02/$ - see front matter
PII: S0022-328X(02)01579-6

been synthesized and spectroscopically characterized [5]. Depending on the redox state, three different valence structures are possible for these even-carbon complexes, which differ by two electron increments and the number of bonds between the terminal carbons and end groups, i.e. $L_mM{-}(C{\equiv}C)_y{-}ML_m$, $L_mM{=}(C{=}C)_y{=}ML_m$ and $L_mM{\equiv}(C{-}C)_y{\equiv}ML_m$.

Very few compounds have been synthesized with an odd number of carbons in the C_x bridge with a length greater than one [22–24] and only non-symmetrical examples are known. This is mainly due to synthetic difficulties, the chain assembling being much easier by coupling of C≡C building blocks which leads only to even numbered bridges. For these odd-carbon complexes two different valence structures are possible; a symmetrical cumulenic structure $L_mM{=}C{=}(C{=}C)_y{=}M'L'_{m'}$, and a unsymmetrical polyynyl/carbyne structure $L_mM{-}(C{=}C)_y{-}C{=}M'L_{m'}$ with a metal–carbon single bond on one end and a metal–carbon triple bond on the other. Gladysz reported the synthesis of mixed metal complexes of the type $[Cp^*Re(NO)(PPh_3)(C_3)M(CO)_a(\eta^5\text{-}C_6H_cCl_{5-c})_b]^+BF_4^-$ (M/*a*/*b*/*c* = Mn/2/1/5, Mn/2/1/4, Mn/2/1/0, Fe/4/0/0) and $[Cp^*Re(NO)(PPh_3)(C_5)Mn(CO)_2(\eta^5\text{-}C_5Cl_5)]^+BF_4^-$ [22], whose spectroscopic and structural features show a prevalent cumulenic structure. Templeton has reported and spectroscopically characterized a cumulated C_3 system, $2K^+[Tp'(CO)_2Mo(=C=C=C=)W(CO)_2Tp']^{2-}$, which can be oxidized to the isolable alkynyl/carbyne species $[Tp'(CO)_2Mo(-C{\equiv}C-C{\equiv})W(CO)_2Tp']$ [23]. The only other alkynyl/carbyne C_3 complex was recently reported by Gladysz and coworkers [24], who synthesized and structurally characterized the $[(\eta^5\text{-}C_5Me_5)Re(NO)(PPh_3)(-C{\equiv}C-C{\equiv})W(O\text{-}t\text{-}Bu)_3]$ species. Few theoretical investigations have been performed on even μ-C_x complexes [25–31], and only one has been very recently carried out on odd carbon bridges [32]. In that paper structure, bonding and metal–metal interactions; in some complexes $[L_yMC_xM'L'_{y'}]^{z+}$ with odd carbon chains have been investigated at the B3LYP density functional level of theory. Ground states with dominant M=(C=C)=C=M character have been found for the symmetrical complexes $[(\eta^5\text{-}C_5H_5)(CO)_2MC_xM(CO)_2(\eta^5\text{-}C_5H_5)]$ with M = Mn, Re, while M–(C≡C)–C≡M′ character has been found for unsymmetrical $[(\eta^5\text{-}C_5H_5)(NO)(PH_3)ReC_3W(OCH_3)_3]$ and $[(\eta^5\text{-}C_5H_5)(NO)(PH_3)ReC_xRe(CO)_2(\eta^5\text{-}C_5H_5)]^+$ complexes. However, that work has essentially focused on the experimental rhenium–manganese and rhenium–tungsten systems and no systematic study on the dependence of the dominant resonance form from the metal electron count has been performed.

In a previous paper [28], we carried out DFT calculations on some model compounds of the even C_x bridged complexes mentioned above which allowed us to clarify the electronic structure, to point out the factors determining the geometric structure (i.e. cumulenic vs. alternating single and triple bonds), to investigate the effect of lengthening the carbon chain and to study the electron delocalization across the wire-like C_x bridges and the metal–metal interaction between them. Herein, we address a general theoretical study on the odd C_x bridged complexes. For these complexes a polyynic structure is possible only if different transition metals are linked. To account for this possibility, DFT LCAO calculations have been performed on a series of $[\{Cp(CO)_2M\}(\mu\text{-}C_x)\{Cp(CO)_2M'\}]$ heterometallic complexes with $x = 3$, 5, 7 and M = Cr, M′ = Fe or M = Fe^+, M′=Mn and $x = 3$, and on the corresponding homometallic complexes with $x = 3$, 5, 7 and M = M′ = Mn or $x = 3$ and M = M′ = Cr, Fe^+. These models of the investigated odd μ-C_x bridged complexes where metal is bound to π-acceptor ligands in a pseudo-octahedral coordination are illustrated in Fig. 1. The move from Cr to Fe allowed us to investigate both the effect of the change of the nature of the transition metal and of the variation of the fragment d configuration. These calculations allowed us: (i) to point out the factors which determine the alternative structure of these complexes, i.e. cumulenic for homometallic series versus alternating single and triple bonds for heterometallic one; (ii) to study the different behavior of complexes with an even number of bridging carbon atoms and those with an odd number; (iii) to investigate the effect of lengthening the carbon chain in both kind of complexes; (iv) to study the electron delocalization across the wire-like C_x bridges and the metal–metal interaction between them.

Among the main results, we have found optimized structures consistent with the experimentally characterized geometries, giving a rationale for their occurrence in terms of the electron count on the metal fragments.

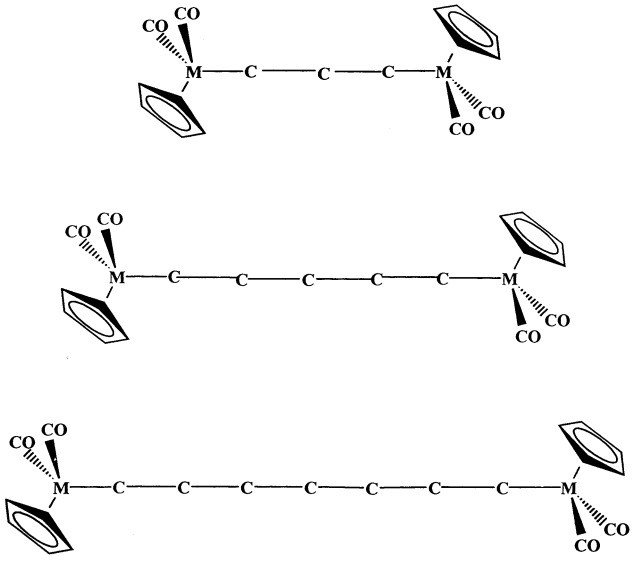

Fig. 1. Geometrical structures of the model complexes.

2. Computational and methodological details

The calculations reported in this paper are based on the Amsterdam Density Functional (ADF) program package described elsewhere [33–35]. Its main characteristics are the use of a density fitting procedure to obtain accurate Coulomb and exchange potentials in each SCF cycle, the accurate and efficient numerical integration of the effective one-electron Hamiltonian matrix elements and the possibility to freeze core orbitals. The molecular orbitals were expanded in an uncontracted double-ζ STO basis set for all atoms with the exception of the transition metal orbitals for which we used a double-ζ STO basis set for 3s and 3p and a triple-ζ STO basis set for 3d and 4s. As polarization functions, one 4p, one 3d and one 2p STO were used for transition metals, O and C, and H, respectively. The cores (Cr, Mn, Fe:1s–2p; C, O: 1s) have been kept frozen.

The LDA exchange correlation potential and energy were used, together with the Vosko–Wilk–Nusair parametrization [36] for homogeneous electron gas correlation, including the Becke's non-local correction [37] to the local exchange expression and the Perdew's non-local correction [38] to the local expression of correlation energy (NLDA). In order to save computer time and to simplify the analysis of the results, molecular structures were optimized by the NLDA method in C_{2h} (or C_s) symmetry.

3. Results and discussion

3.1. A qualitative Hückel-type model

We propose here a simple molecular orbital scheme for $(x+2)$-center M–C_x–Mπ and δ interactions with odd C_x, which is an extension of that employed for even chain C_x complexes [28,29,39]. The assumptions on which this model is based will be justified in the next paragraph on the basis of the accurate DFT calculations. In such a model, we assume that the energy order of the bridging orbitals, classified on the basis of their symmetry with respect to the M–C_x–M axis (assumed to be the z axis), is $\sigma \ll \pi \leq \delta \leq \delta^* \leq \pi^* \ll \sigma^*$. The σ skeleton is therefore neglected and only the interactions of the carbon π with the metal d_π-orbitals, originating the uppermost frontier orbitals involved in the bonding of the C_x bridge, are considered and built within a simple Hückel-type approach. Assuming comparable energies for the C p_π and the M d_π orbitals, the π-system is constituted by the $(x+2)$-center molecular orbitals qualitatively illustrated in Scheme 1 for $x = 3$.

The energy diagram is, therefore, made up by $(x+2)$ closely spaced couples of levels (C_{2h} symmetry or lower), obtained by linear combinations of M d_{xz}, C p_x or M d_{yz}, C p_y orbitals, whose energies increase with increasing nodal planes and which are designated as $1\pi-(x+2)\pi$. The orbitals of δ symmetry built by the bonding and antibonding combinations of the d_{xy}, and eventually also of the $d_{x^2-y^2}$ orbitals, depending on the co-ordination geometry of the L_mM fragment, complete the overall scheme. These orbitals give no contribution to the bonding, as they do not interact with any C_x orbital; they will be designated as 1δ–4δ and should lie between 1π and $(x+2)\pi$. Both the metal character of the $1\pi-(x+2)\pi$ orbitals and the relative position of the 1δ–4δ levels are determined by the nature of the metals and of the ligands and by the co-ordination geometry in the metal fragments. Regarding the σ M–C_x–M skeleton as mainly constant, the variation in the M–C and C–C bond character can be attributed to changes in the nature and in the occupancy of the π-frontier orbitals. As for as the occupancy of these levels, it is convenient to perform the electron count by considering a neutral C_x molecule bracketed by the two metal ML_m fragments. On this basis the d^n configuration attributed to the ML_m fragment does not take into account the bond with the carbon atom and is at least one unit higher than that attributable to the metal in the whole complex according to the conventional oxidation state assignment. If each L_mM fragment has a d^n configuration, a total of $2(n-1)+2x$ electrons are left to occupy these π and δ frontier orbitals: $2x$ coming from the C_x unit and $(n-1)$ from each metal fragment, as one is employed in the M–C σ bond. A relevant difference between systems with an even bridge and those with an odd one arises when these electrons are distributed on the π-orbitals.

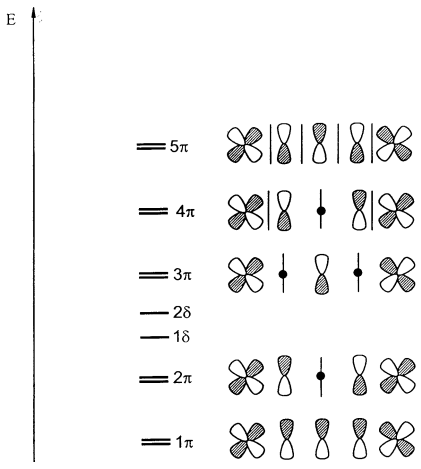

Scheme 1.

Let us consider an odd bridging chain taking as an example a $L_mMC_3ML_m$ complex with the metal in a pseudo-octahedral co-ordination. The energy level diagram foreseen for the π–δ system of this complex is illustrated in Scheme 1. To distinguish the carbon atoms along the chain, we will use Greek letters beginning from

the first carbon atom on the left, i.e. M–C_α–C_β–C_γ···M. Note that for the pseudo-octahedral co-ordination of the metal fragment the $d_{x^2-y^2}$ levels are destabilized by σ-interactions with the ligands, leaving only two δ levels at energies close to that of the 3π orbital (see Scheme 1). For metal fragments with a d^6 configuration, these orbitals should be filled with 16 electrons and the HOMO is the 3π one. The molecular geometry is mainly determined by the nodal pattern of such a HOMO which shows two nodal planes bisecting exactly the outer C_α and C_γ carbons and is essentially non-bonding. These nodes could suggest a cumulene-like structure. For metal fragments with a d^5 configuration, like $[Cp(CO)_2Cr]$, the HOMO is only half filled so that the geometry is not expected to change from the cumulene-like structure. For metal fragments with a d^7 configuration, like $[Cp(CO)_2Fe]$, having the HOMO 4π half filled, a geometry close to a cumulene-like structure is again expected. However, for metal fragments with a d^5 or a d^7 configuration, a triplet ground state could be predicted and, therefore, these species should be unstable and reactive. Analogous arguments apply to longer odd carbon chains making use of the topology of Hückel orbitals. For a $L_mMC_xML_m$ complex based on metal fragments with a d^6 configuration, the HOMO is the $(x+3)/2$ π-orbital which has $(x+1)/2$ nodes bisecting the carbon atoms localized in the odd positions along the chain (C_α, C_γ, …), as shown in Scheme 2.

Taking into account that (i) the HOMO is symmetric (S) or antisymmetric (A) with respect to the bisecting plane depending on the value of $(x+2)$mod 4, S if $(x+2)$mod 4 is 1, A if $(x+2)$mod 4 is 3; (ii) the nodes must be as distributed as possible, we can predict the nodal pattern illustrated in Scheme 2. This nodal pattern suggests a cumulene-like geometry which is foreseen not to change substantially by adding or subtracting two electrons in complexes based on d^7 and d^5 metal fragments, respectively. Due to the nodal pattern of the π-orbitals characterized by the presence of a number of nodes bisecting carbon atoms instead of C–C and M–C bonds, it is difficult to assign definite valence structures to these species with an odd number of carbon chains. However, the above analysis gives evidence of a special stability of the $L_mMC_xML_m$ complexes with x odd based on metal fragments with a d^6 configuration. Note that this configuration corresponds to a total number of electrons of $2x+10$ in the π–δ system ($2x+6$ in the π system). Although all the experimentally known complexes with an odd number of carbons in the chain are heteronuclear species based on different metal fragments, i.e. $L_mM(\mu\text{-}C_x)M'L'_{m'}$, those with mid to late transition metals in low oxidation states and pseudooctahedral coordination [22,23] do have the total number of electrons indicated above. For these heteronuclear complexes the nodal pattern of the π-orbitals is modified as a consequence of the different electronegativity of the two metal fragments which breaks the symmetry of these systems. Moreover, it is possible to demonstrate that the nodal planes do not bisect the carbon atoms anymore but the C–C and M–C bonds, moving and localizing toward the most electronegative metal fragment, as shown in Scheme 3 for a general $L_mMC_xM'L'_{m'}$ complex.

For metal fragments L_mM and $L'_{m'}M'$ with a total of 12 d electrons (typically d^6/d^6 or d^5/d^7), the $(x+3)/2$ π-orbital represents the fully occupied HOMO. Its nodal pattern suggests a partial alkynyl/carbyne geometry, with a triple bond between the least electronegative metal fragment and the adjacent carbon and a single bond between the most electronegative metal fragment and the adjacent carbon. Therefore, $L_mM(\mu\text{-}C_x)M'L'_{m'}$ complexes are described by both cumulenic and alkynyl/carbyne resonance forms, the contribution of the alkynyl/carbyne form being the higher the larger is the difference between the electron-attracting properties of the ML_m and $M'L'_{m'}$, metal fragments.

3.2. DFT calculations on the $[\{Cp(CO)_2M\}(\mu\text{-}C_x)\{Cp(CO)_2M'\}]$ series

The ground states and the configurations of the considered complexes with C_3, C_5 and C_7 chains are reported in Table 1. For the considered complexes with

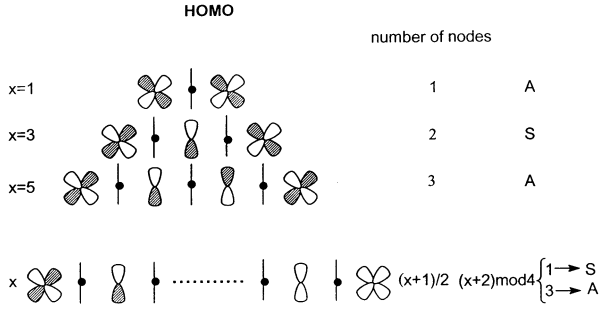

Scheme 2.

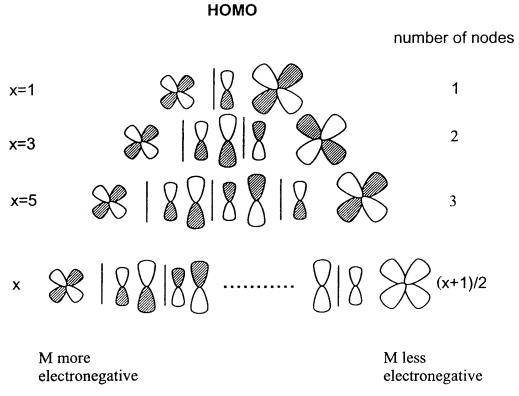

Scheme 3.

Table 1
Metal d^n configurations, complex configurations electronic states and energies (with respect to atoms) for the homometallic chromium, manganese, dicationic iron complexes and for the heterometallic iron–chromium and iron–manganese monocationic complexes

Complex	Metals d configuration	Complex configuration	State	Energy (eV)
$[\{Cp(CO)_2Cr\}_2(\mu\text{-}C_3)]$	d^5/d^5	$(21b_u)^1(13a_u)^1$	^3B_g	−226.75
$[\{Cp(CO)_2Cr\}_2(\mu\text{-}C_3)]$	d^5/d^5	$(21b_u)^2(13a_u)^0$	^1A_g	−227.10
$[\{Cp(CO)_2Mn\}_2(\mu\text{-}C_3)]$	d^6/d^6	$(21b_u)_2(13a_u)^2$	^1A_g	−228.69
$[\{Cp(CO)_2Fe\}_2(\mu\text{-}C_3)]^{+2}$	d^6/d^6	$(21b_u)^2(13a_u)^2$	^1A_g	−210.40
$[\{Cp(CO)_2Fe\}(\mu\text{-}C_3)\{Cp(CO)_2Cr\}]$	d^7/d^5	$(25a'')^2(41a')^2$	$^1A'$	−227.16
$[\{Cp(CO)_2Fe\}(\mu\text{-}C_3)\{Cp(CO)_2Mn\}]^+$	d^6/d^6	$(25a'')^2(41a')^2$	$^1A'$	−221.36
$[\{Cp(CO)_2Mn\}_2(\mu\text{-}C_5)]$	d^6/d^6	$(22a_g)^2(13b_g)^2$	^1A_g	−244.62
$[\{Cp(CO)_2Mn\}_2(\mu\text{-}C_7)]$	d^6/d^6	$(24b_u)^2(14a_u)^2$	^1A_g	−260.56
$[\{Cp(CO)_2Fe\}(\mu\text{-}C_5)\{Cp(CO)_2Cr\}]$	d^7/d^5	$(26a'')^2(44a')^2$	$^1A'$	−243.19
$[\{Cp(CO)_2Fe\}(\mu\text{-}C_7)\{Cp(CO)_2Cr\}]$	d^7/d^5	$(27a'')^2(47a')^2$	$^1A'$	−259.20

an odd chain, the ground state is always a singlet, ^1A_g or $^1A'$, whatever the d^n configuration of the metal fragment. We have calculated a triplet excited state (^3B_g) for d^5 configuration of the chromium homonuclear complex which is 0.35 eV higher than the singlet. Table 2 shows the main optimized geometrical parameters of the $[\{Cp(CO)_2M\}(\mu\text{-}C_3)\{Cp(CO)_2M'\}]$ $M = M' = Cr$, Mn, Fe^+ homonuclear series of complexes and the M = Fe, $M' = Cr$ and $M = Fe^+$, $M' = Mn$ heteronuclear series of complexes. The main optimized geometrical parameters of the $[\{Cp(CO)_2Mn\}_2(\mu\text{-}C_x)$ $x = 3$, 5, 7 series, the corresponding HOMO–LUMO gaps, HOMO energies and HOMO metal character are shown in Table 3, while the optimized geometrical parameters, the HOMO–LUMO gaps, HOMO energies and HOMO metal character of the $[\{Cp(CO)_2Fe\}(\mu\text{-}C_x)\{Cp(CO)_2Cr\}]$, $x = 3$, 5, 7 species are shown in Table 4. The species $[\{Cp(CO)_2Mn\}_2(\mu\text{-}C_3)]$ and $[\{Cp(CO)_2Fe\}(\mu\text{-}C_3)\{Cp(CO)_2Cr\}]$ are stable closed shell singlets and while the homonuclear species show the highest HOMO–LUMO gap in the manganese series ($x = 3$, 5, 7), the heteronuclear species show the lowest HOMO–LUMO gap in the iron–chromium series ($x = 3$, 5, 7) and their MO diagrams will serve as a basis for the discussion of all the other complexes. The computed valence energy levels of the manganese and iron–chromium C_3 dimers, labeled according to C_{2h} and C_s symmetries, are reported in Tables 5 and 6, respectively (for the C_5 and C_7 dimers use supplementary material). The orbitals of main metal or C_x character are classified on the basis of their symmetry with respect to the $M–C_x–M$ axis (the y axis) in σ, π, δ, σ*, π* and δ*.

Table 2
Main optimized geometrical parameters of the $[\{Cp(CO)_2M\}\{Cp(CO)_2M'\}(\mu\text{-}C_3)]$ complexes, homonuclear $M = M' = Cr$, Mn, Fe^+ and heteronuclear M = Fe, $M' = Cr$ and $M = Fe^+$, $M' = Mn$

Compound	Parameter	NLDA (Å °)
$[\{Cp(CO)_2Cr\}_2(\mu\text{-}C_3)]$ (^3B_g)	$Cr–C(C_3)$	1.797
	$C_\alpha–C_\beta$	1.294
	$C_\beta–C_\gamma$	1.294
	$Cr–C_\alpha–C_\beta$	173.1
$[\{Cp(CO)_2Cr\}_2(\mu\text{-}C_3)]$ (^1A_g)	$Cr–C(C_3)$	1.804
	$C_\alpha–C_\beta$	1.293
	$C_\beta–C_\gamma$	1.293
	$Cr–C_\alpha–C_\beta$	171.9
$[\{Cp(CO)_2Mn\}_2(\mu\text{-}C_3)]$	$Mn–C(C_3)$	1.776
	$C_\alpha–C_\beta$	1.287
	$C_\beta–C_\gamma$	1.287
	$Mn–C_\alpha–C_\beta$	175.0
$[\{Cp(CO)_2Fe\}_2(\mu\text{-}C_3)]^{+2}$	$Fe–C(C_3)$	1.759
	$C_\alpha–C_\beta$	1.281
	$C_\beta–C_\gamma$	1.281
	$Fe–C_\alpha–C_\beta$	177.5
$[\{Cp(CO)_2Fe\}\{Cp(CO)_2Cr\}(\mu\text{-}C_3)]$	$Fe–C_\alpha(C_3)$	1.878
	$Cr–C_\gamma(C_3)$	1.728
	$C_\alpha–C_\beta$	1.242
	$C_\beta–C_\gamma$	1.346
	$Fe–C_\alpha–C_\beta$	176.4
	$Cr–C_\gamma–C_\beta$	172.5
	$C_\alpha–C_\beta–C_\gamma$	179.9
$[\{Cp(CO)_2Fe\}\{Cp(CO)_2Mn\}(\mu\text{-}C_3)]^{+1}$	$Fe–C_\alpha(C_3)$	1.826
	$Mn–C_\gamma(C_3)$	1.718
	$C_\alpha–C_\beta$	1.255
	$C_\beta–C_\gamma$	1.315
	$Fe–C_\alpha–C_\beta$	177.6
	$Mn–C_\gamma–C_\beta$	175.1
	$C_\alpha–C_\beta–C_\gamma$	179.9

The electronic interaction between the odd C_x unit and the metal fragments can be investigated by considering a fragment approach in which the two $[Cp(CO)_2M]$ and $[Cp(CO)_2M']$ fragments interact with a C_x species along a common MC_xM' axis, and, therefore, by employing the same electron count used in the Hückel-like model. The $[Cp(CO)_2M]$ M = Cr, Mn, Fe fragments have been considered in a pseudo-octahedral structure, of C_s symmetry, with the same geometries obtained by the optimization of the corresponding dinuclear complexes, and their main valence orbitals are reported in Fig. 2. The frontier d orbitals split into a lower set of three t_{2g}-like orbitals, labeled as $17a'(d_{z^2})$, $12a''(d_{yz})$ and $18a'(d_{xy})$ in the C_s point group, and a higher set of e_g-like orbitals, labeled as $19a'(d_{x^2-y^2})$ and

Table 3
Main optimized geometrical parameters, HOMO–LUMO gaps, HOMO energies, e, and HOMO metal character, M (%), for [{Cp(CO)$_2$Mn}$_2$(μ-C$_x$)] complexes, $x = 3, 5, 7$

Compound	Parameter	NLDA (Å °)	HOMO–LUMO gap (eV)	e (HOMO) (eV)	M (%)
[{Cp(CO)$_2$Mn}$_2$(μ-C$_3$)]	Mn–C(C$_3$)	1.776	2.067	−5.35	62
	C$_\alpha$–C$_\beta$	1.287			
	C$_\beta$–C$_\gamma$	1.287			
	Mn–C$_\alpha$–C$_\beta$	175.0			
	C$_\alpha$–C$_\beta$–C$_\gamma$	180.0			
[{Cp(CO)$_2$Mn}$_2$(μ-C$_5$)]	Mn–C(C$_5$)	1.780	1.544	−5.42	46
	C$_\alpha$–C$_\beta$	1.283			
	C$_\beta$–C$_\gamma$	1.283			
	C$_\gamma$–C$_\delta$	1.283			
	C$_\delta$–C$_\varepsilon$	1.283			
	Mn–C$_\alpha$–C$_\beta$	174.4			
	C$_\alpha$–C$_\beta$–C$_\gamma$	178.8			
	C$_\beta$–C$_\gamma$–C$_\delta$	180.0			
[{Cp(CO)$_2$Mn}$_2$(μ-C$_7$)]	Mn–C(C$_7$)	1.776	1.238	−5.48	43
	C$_\alpha$–C$_\beta$	1.282			
	C$_\beta$–C$_\gamma$	1.282			
	C$_\gamma$–C$_\delta$	1.276			
	C$_\delta$–C$_\varepsilon$	1.276			
	C$_\varepsilon$–C$_\zeta$	1.282			
	C$_\zeta$–C$_\eta$	1.282			
	Mn–C$_\alpha$–C$_\beta$	174.3			
	C$_\alpha$–C$_\beta$–C$_\gamma$	178.0			
	C$_\beta$–C$_\gamma$–C$_\delta$	178.9			
	C$_\gamma$–C$_\delta$–C$_\varepsilon$	180.0			

13a″(d_{xz}). One of the two d_δ orbitals (17a′) lies at low energies because is stabilized by the backbonding to the CO π*, while the other one (13a″) lies at high energies due to the interactions with the CO 5σ. The d_π orbitals, 18a′ and 12a″, are almost degenerate and are stabilized by the backbonding to the CO π*. The 19a′ is a d_σ, orbital (dsp hybrid) and is singly occupied in the iron fragment. The C_x molecules ($x = 3, 5, 7$) have been considered in a singlet state, with bond distances and angles (the chain is slightly bent) equal to those found in the corresponding dinuclear complexes. The main valence orbitals are reported on the right in Fig. 3 for C_3. In each case, the doubly occupied HOMO orbitals, $2a_g$ and $3b_u$ for C_3 (denoted $2\sigma_g$ and $2\sigma_u$, respectively, in Fig. 3), $4a_g$ and $4b_u$ for C_5, and, finally, $5a_g$ and $6b_u$ for C_7 in C_{2h} symmetry, correspond to the in-phase and out-of-phase combinations of the terminal carbon sp hybrids and are of the right symmetry to interact with the metal d_σ orbitals. The HOMOs $1a_u$, $2b_u$ ($1\pi_u$) for C_3, $3a_g$, $1b_g$ ($1\pi_g$) for C_5, and $5b_u$ $2a_u$, ($2\pi_u$) for C_7 correspond to the two highest occupied orthogonal π-orbitals, while the LUMOs $3a_g$, $1b_g$ ($1\pi_g$) for C_3, $2a_u$, $5b_u$ ($2\pi_u$) for C_5, and $2b_g$, $6a_g$ ($2\pi_g$) for C_7 correspond to the two lowest π*-orbitals. Fig. 3 shows the orbital interaction diagram for the [{Cp(CO)$_2$M}$_2$(μ-C$_3$)] complex which is representative of the behavior in the homonuclear series [{Cp(CO)$_2$M}$_2$(μ-C$_x$)] $x = 3, 5, 7$. In this figure we report the energy levels for the metal fragments at the same distance observed in the whole complex, which, due to extremely small interactions between the two fragments, consists of almost degenerate symmetric and antisymmetric combinations of the levels for the single fragment. In all of these complexes, the orbitals describing the interactions between metal atoms and the bridging C_x, $x = 3, 5, 7$ moiety can be divided into five groups: (i) two low-lying orbitals describing the σ M–C bonds and $(x-1)$ lower-lying orbitals describing the C–C σ bonds, not shown in the figure, which constitute the M–C$_x$–M σ skeleton; (ii) a group of closely spaced couples of levels originating from the interactions of the $C_x p_\pi$ with the metal d_π orbitals; (iii) a few orbitals of δ symmetry built by the bonding and antibonding combinations of the d_{z^2} and d_{xz}, strongly mixed with ligand orbitals, which do not interact with any $C_x p_\pi$ orbital and give no contribution to the bonding; (iv) a group of high lying occupied orbitals describing the M–Cp interactions; (v) a group of low-lying virtual orbitals which are essentially of d_δ–π*(CO) and d_δ–π*(Cp) character.

These results show that the calculated frontier orbitals of manganese species correspond closely those of the proposed Hückel-like model (see above). In particular, a careful analysis of the levels originating from the interactions of the $C_x p_\pi$ with the metal d_π orbitals shows the same nodal pattern and the same energy order expected on the basis of such a model. Moreover, an analysis of the composition of these π-orbitals (see Table 5) shows that the 1π-orbitals have an almost pure $1a_u$/

Table 4
Main optimized geometrical parameters, HOMO–LUMO gaps, HOMO energies, e, and HOMO metal character, M (%), for [{Cp(CO)$_2$Fe}{Cp(CO)$_2$Cr}(μ-C$_x$)] complexes, $x = 3, 5, 7$

Compound	Parameter	NLDA (Å °)	HOMO–LUMO gap (eV)	e (HOMO) (eV)	M (%)
[{Cp(CO)$_2$Fe}{Cp(CO)$_2$Cr}(μ-C$_3$)]	Fe–C$_\alpha$(C$_3$)	1.878	1.023	−4.78	52(Cr)
	Cr–C$_\gamma$(C$_3$)	1.728			
	C$_\alpha$–C$_\beta$	1.242			
	C$_\beta$–C$_\gamma$	1.346			
	Fe–C$_\alpha$–C$_\beta$	176.4			
	Cr–C$_\gamma$–C$_\beta$	172.5			
	C$_\alpha$–C$_\beta$–C$_\gamma$	179.9			
[{Cp(CO)$_2$Fe}{Cp(CO)$_2$Cr}$_2$(μ-C$_5$)]	Fe–C$_\alpha$(C$_5$)	1.878	1.115	−4.99	52(Cr)
	Cr–C$_\varepsilon$(C$_5$)	1.734			
	C$_\alpha$–C$_\beta$	1.238			
	C$_\beta$–C$_\gamma$	1.329			
	C$_\gamma$–C$_\delta$	1.245			
	C$_\delta$–C$_\varepsilon$	1.330			
	Fe–C$_\alpha$–C$_\beta$	174.3			
	C$_\gamma$–C$_\varepsilon$–C$_\delta$	172.1			
	C$_\alpha$–C$_\beta$–C$_\gamma$	177.5			
	C$_\beta$–C$_\gamma$–C$_\delta$	179.5			
	C$_\gamma$–C$_\delta$–C$_\varepsilon$	178.5			
[{Cp(CO)$_2$Fe}{Cp(CO)$_2$Cr}(μ-C$_7$)]	Fe–C$_\alpha$(C$_7$)	1.879	1.166	−5.15	53(Cr)
	C$_\gamma$–C$_\eta$(C$_7$)	1.738			
	C$_\alpha$–C$_\beta$	1.239			
	C$_\beta$–C$_\gamma$	1.330			
	C$_\gamma$–C$_\delta$	1.241			
	C$_\delta$–C$_\varepsilon$	1.315			
	C$_\varepsilon$–C$_\zeta$	1.250			
	C$_\zeta$–C$_\eta$	1.324			
	Fe–C$_\alpha$–C$_\beta$	174.8			
	Cr–C$_\eta$–C$_\zeta$	172.5			
	C$_\alpha$–C$_\beta$–C$_\gamma$	177.5			
	C$_\beta$–C$_\gamma$–C$_\delta$	179.4			
	C$_\gamma$–C$_\delta$–C$_\varepsilon$	179.7			
	C$_\delta$–C$_\varepsilon$–C$_\zeta$	179.1			
	C$_\varepsilon$–C$_\zeta$–C$_\eta$	178.4			

2b$_u$, 3b$_u$/1a$_u$ or 4b$_u$/1a$_u$ (C$_3$, C$_5$ or C$_7$) character and only the highest occupied π-orbitals have a substantially mixed metal–carbon character. The assumption of the qualitative Hückel model, according to which the occupation of the highest molecular orbital of π character determines the valence description of the M–C and C–C bonds is thus justified. Fig. 4 shows the orbital interaction diagram of [{Cp(CO)$_2$Fe}(μ-C$_3$){Cp(CO)$_2$Cr}] complex which is representative of the behavior in the heterometallic series [{Cp(CO)$_2$M}(μ-C$_x$){Cp(CO)$_2$M′}] $x = 3, 5, 7$. The orbitals describing the interaction between metal atoms and the bridging C$_x$ $x = 3, 5, 7$ moiety can be divided into essentially the same groups above mentioned for the homonuclear manganese series. However, two major differences arise if we compare the composition of the π-orbitals and the π–δ energy order (see Table 6) with those of the homonuclear complexes:

i) the low-lying π levels originate from the interaction of the $C_x p_\pi$ with the iron (more electronegative) d$_\pi$ orbitals, while the highest occupied and the unoccupied π-orbitals have a substantially chromium (less electronegative) carbon character;
ii) the HOMO orbital is a δ symmetry level built by the chromium d$_{z^2}$, with the corresponding δ orbital (d$_{z^2}$) localized on iron lying much lower, while the LUMO is a δ symmetry orbital built by the iron d$_{xz}$. The occupation of the molecular orbitals of π character with nodal planes mostly localized between iron and carbon determines the valence description of the M–C, M′–C and C–C bonds, in agreement with the proposed Hückel–lyke model (see above).

4. Geometries

The calculated C–C and M–C bond distances in the homonuclear [{Cp(CO)$_2$M}$_2$(μ-C$_x$)], ($x = 3, 5, 7$, M = Cr, Mn, Fe$^+$) and heteronuclear [{Cp(CO)$_2$Fe}(μ-C$_x$){Cp(CO)$_2$Cr}] ($x = 3, 5, 7$) series, including the

Table 5
Energies and composition of the $[\{Cp(CO)_2Mn\}_2(\mu\text{-}C_3)]$ lowest unoccupied and highest occupied orbitals

Orbital	e (eV)	Mn (%)	CO (%)	Cp (%)	C_3 (%)
$22b_u$	−2.19	37 ($3d_{x^2-y^2}$)	15		
$14b_g$ (4δ)	−2.22	42 ($3d_{xz}$)	13	14	
$22a_g$	−2.24	43 ($3d_{x^2-y^2}$)	10		
$14a_u$ (3δ)	−2.40	34 ($3d_{xz}$)+12 ($3d_{yz}$)	11	13	
$13b_g$ (4π)	−3.04	33 ($3d_{yz}$)			49
$2la_g$ LUMO (4π)	−3.29	19 ($3d_{xy}$)			66
13_a HOMO (3π)	−5.35	18 ($3d_{xz}$)+44 ($3d_{yz}$)			15
$21b_u^u$ (3π)	−5.73	19 ($3d_{x^2-y^2}$)+43 ($3d_{xy}$)			10
$20a_g$ (2δ)	−6.04	49 ($3d_{z^2}$)+7 ($3d_{x^2-y^2}$)			
$20b_u$ ($l\delta$)	−6.10	52 ($3d_{z^2}$)			
$19a_g$ (2π)	−6.72	43 ($3d_{xy}$)			14
$12b_g$ (2π)	−6.75	19 ($3d_{xz}$)+29 ($3d_{yz}$)			32
$19b_u$	−7.40			52	
$12a_u$	−7.74	16 ($3d_{yz}$)		62	
$11b_g$	−7.74	17 ($3d_{yz}$)		61	
$18a_g$	−7.82	23 ($3d_{x^2-y^2}$)		39	
$11a_u$ (1π)	−8.55				85
$18b_u$ (1π)	−8.73				67
$17b_u$ (σ)	−9.51	11 ($3d_{xy}$)+9 ($3d_{x^2-y^2}$)			36
$17a_g$ (σ)	−9.98	3 ($3d_{x^2-y^2}$)+8 ($3d_{xy}$)		35	34

Only the main contributions to each orbital have been given. The nature of metal contributions is mentioned in parentheses as well as the σ, π and δ nature of MOs.

$[\{Cp(CO)_2Fe\}(\mu\text{-}C_3)\{Cp(CO)_2Mn\}]^+$ complex, are reported in Tables 2–4. All calculated geometrical parameters match very well with the model previously proposed, with the d^5, d^6 and d^7 configurations of the $[Cp(CO)_2M]$ metal fragments leading to cumulenic valence descriptions for the homometallic complexes. An essentially cumulenic structure has been obtained for the monocationic C_3 complex of manganese and iron, whose C–C, M′–C and M–C bond lengths reproduce those observed for the corresponding experimentally synthesized complex $[Cp^*Re(NO)(PPh_3)(\mu\text{-}C_3)Mn(CO)_2Cp]^+$ with the same d^6/d^6 metal configuration [22]. All heteronuclear iron–chromium C_x bridged (x = 3, 5, 7) complexes show essentially polyynic structures, with alternating triple and single bonds, starting from a single Fe–C bond and ending with a triple Cr–C bond. Table 2 illustrates that going from Cr to Fe^+ in the $[\{Cp(CO)_2M\}_2(\mu\text{-}C_3)]$ series, i.e. going from a d^5 to a d^6

Table 6
Energies and composition of the $[\{Cp(CO)_2Fe\}\{Cp(CO)_2Cr\}(\mu\text{-}C_3)]$ lowest unoccupied and highest occupied orbitals

Orbital	e (eV)	Fe (%)	Cr (%)	CO (%)	Cp (%)	C_3 (%)
27a″ (4π)	−2.42		19 ($3d_{yz}$)	10		39
44a′	−2.44	11 ($3d_{z^2}$)		44		
43a′ (4π)	−2.78		14 ($3d_{xy}$)			32
42a′	−3.46	35 ($3d_{x^2-y^2}$)				
26a″ LUMO (3δ)	−3.76	30 ($3d_{xz}$)+15 ($3d_{yz}$)		12	15	
41a′ HOMO (2δ)	−4.78		52 ($3d_{z^2}$)	17		
25a″ (3π)	−5.20		11 ($3d_{xz}$)+25 ($3d_{yz}$)			29
40a′ (3π)	−5.39		37 ($3d_{xy}$)			21
39a′	−6.61		8 ($3d_{x^2-y^2}$)		55	
24a″	−6.81		11 ($3d_{yz}$)		64	
23a″ (2π)	−6.99	17 ($3d_{xz}$)+27 ($3d_{yz}$)				29
38a′ (1δ)	−7.12	16 ($3d_{z^2}$)+16 ($3d_{x^2-y^2}$)+20 ($3d_{xy}$)				
37a′ (2π)	−7.52	30 ($3d_{z^2}$)+12 ($3d_{xy}$)				17
36a′ (1π)	−8.15	13 ($3d_{z^2}$)+16 ($3d_{xy}$)				31
22a″ (1π)	−8.27	9 ($3d_{xz}$)+10 ($3d_{yz}$)				73
21a″	−8.69	19 ($3d_{yz}$)			57	
35a′ (σ)	−8.79	16 ($3d_{x^2-y^2}$)			16	17
34a′ (σ)	−8.94	8 ($3d_{x^2-y^2}$)	8 ($3d_{x^2-y^2}$)+6 ($3d_{xy}$)			29

Only the main contributions to each orbital have been given. The nature of metal contributions is mentioned in parentheses as well as the σ, π and δ nature of MOs.

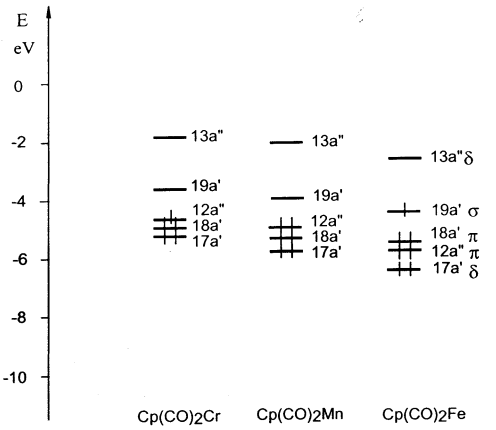

Fig. 2. Energies of the main frontier orbitals for the $[Cp(CO)_2M]$ metal fragments.

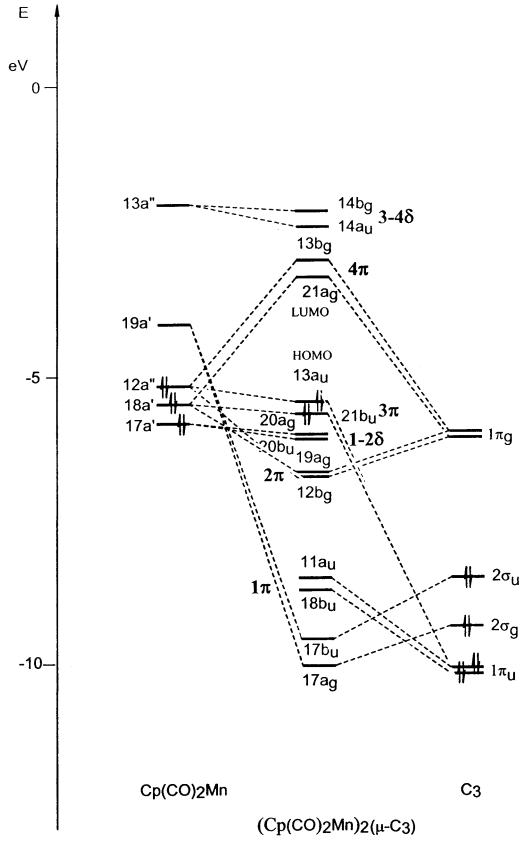

Fig. 3. Molecular orbital diagram for the $[\{Cp(CO)_2Mn\}_2(\mu\text{-}C_3)]$ complex depicting the interactions between the frontier orbitals of $[Cp(CO)_2Mn]$ and C_3.

configuration of the $[Cp(CO)_2M]$ fragment, the C–C bonds remain almost constant. From Tables 3 and 4 we observe the same trend for the $[\{Cp(CO)_2Mn\}_2(\pi\text{-}C_x)]$, $x = 3$, 5, 7 and the $[\{Cp(CO)_2Fe\}(\mu\text{-}C_x)\{Cp(CO)_2Cr\}]$ $x = 3$, 5, 7 series. In particular, we see that the C–C and M–C bond length values do not change on lengthening the C_x bridge. We must take into account that to assign the calculated C–C bond lengths to single, double or

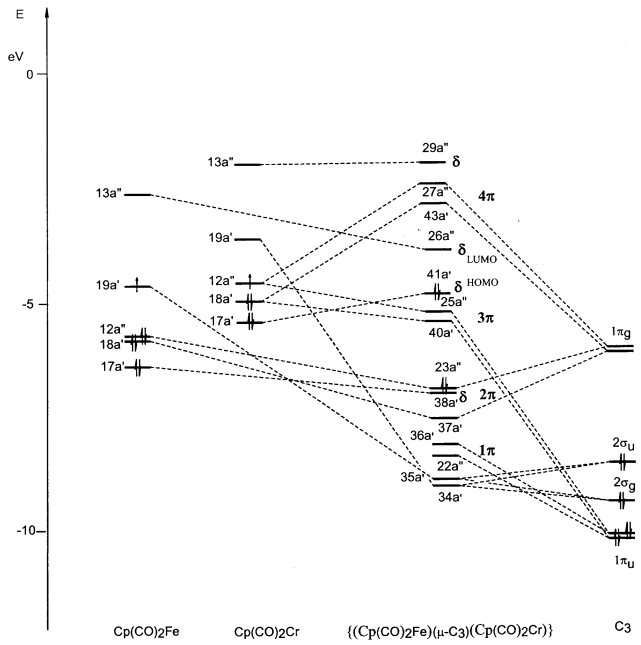

Fig. 4. Molecular orbital diagram for the $[\{Cp(CO)_2Fe\}(\mu\text{-}C_3)\{Cp(CO)_2Cr\}]$ complex depicting the interactions between the frontier orbitals of $[Cp(CO)_2Fe]$ and C_3, and $[Cp(CO)_2Cr]$ and C_3.

triple C–C bonds the right comparison should be made with single, double and triple bonds between sp hybridized carbons. So, for a (MC)···–C≡C–···(CM) triple bond the most, pertinent comparison can be made with ethyne (1.212 Å), for a (MC)···=C=C=···(CM) double bond such a comparison is provided by the central C–C distance in buta-1,2,3-triene (1.284 Å) and for a (MC)···≡C–C≡···(CM) single bond by the central C–C distance in buta-1,2,3-diyne (1.384 Å). Therefore, we assigned carbon–carbon single, double and triple bonds to C–C distances in the range 1.32–1.35, 1.27–1.30 and 1.24–1.25 Å, respectively. More difficult is the assignment of the M–C bond orders on the basis of the optimized M–C bond lengths because of the limited available experimental data. However, we can say that Cr–C bond distance of 1.804 Å is in the range of distances expected for the Cr–C double bonds in the homometallic complex. The Mn–C bond distance of 1.776 Å has a value which can be reasonably assigned to a double bond. The Fe–C bond distance in the dicationic complex of 1.759 Å has a value close to experimentally observed double Fe^+–C bonds (e.g. 1.81 Å in $[(CO)_2CpFe{=}CCl_2]^+$ [40]). For the monocationic, heterometallic complex of iron and manganese (M = Fe^+, M′ = Mn) with $x = 3$, the C–C bond distances (1.255 and 1.315 Å) are very close to those observed for the corresponding experimental system (M = Re, M′ = Mn, $x = 3$) (1.26 and 1.32 Å), the Mn–C bond length (1.718 Å) compares with the experimental value of 1.75 Å, and the Fe^+–C bond length (1.826 Å) can be assigned again to a double bond. This structure has been considered of cumulenic type.

Finally, in Table 4 we show the optimized geometrical parameters of the [{Cp(CO)$_2$Fe}(μ-C$_x$){Cp(CO)$_2$Cr}] $x = 3$, 5, 7. We notice that the C–C bond lengths assume alternating values of 1.24 and 1.33 Å which are close to the values reported for the corresponding hydrocarbons with triple and single C–C bonds, and that on lengthening the C$_x$ chain from $x = 3$ to 7 the C–C bond distances remain almost constant. For instance, for $x = 3$, the Fe–C≡C–C≡Cr carbon–carbon triple bonds (1.242 Å) compare very well with calculated (CH$_3$)C≡C···≡C(CH$_3$) triple bonds (1.222–1.232 Å) and for the C–C single bonds (1.346 Å), they are in good agreement with the calculated (CH$_3$)C≡C···≡C(CH$_3$) single bonds (about 1.34 Å). The Fe–C distance of 1.88 Å is in the range of single Fe–C bonds with a sp hybridized carbon (1.90 Å), while the Cr–C bond distance of 1.73 Å is in the range of distances expected for the Cr–C triple bonds, 1.65–1.79 Å [41].

In order to summarize the results, Lewis formulae for our homo- and heteronuclear model complexes have been written in Scheme 4.

These formulae allow to show explicitly the complexes where metal atoms are 17- or 18-electron centers and where the metal centers have a closed-shell configuration. As we can see, closed-shell metal center configurations can be found both for homo- and heteronuclear complexes, giving rise to cumulenic and polyynyl/carbyne valence structure, respectively, while open-shell configurations can be found for homonuclear complexes, originating a cumulenic valence structure.

5. Metal-chain interactions and bridge length

5.1. Homonuclear series

The orbital interaction diagram in Fig. 3 shows the most relevant interactions between the metal (Mn) fragment d$_\pi$ orbitals and the π system of the C$_3$ bridging unit. We can distinguish two main interactions: (i) a filled–filled interaction between the d$_\pi$ orbitals 18a′ 12a″ and the 1a$_u$/2b$_u$ (1π$_u$) (C$_3$) or 3a$_g$/1b$_g$ (1π$_g$) (C$_5$) or 5b$_u$/2a$_u$ (2π$_u$) (C$_7$) bridge orbitals; and (ii) a filled–empty interaction between the same d$_\pi$ orbitals 18a′ 12a″ and the 3a$_g$/1b$_g$ (1π$_g$) (C$_3$) or 2a$_u$/5b$_u$ (1π$_u$) (C$_5$) or 2b$_g$/6a$_g$ (2π$_g$) (C$_7$) orbitals. The HOMO orbital is composed mainly of the highest occupied bridge orbitals of π symmetry, 1π$_u$, (C$_3$) or 1π$_g$ (C$_5$) or 2π$_u$ (C$_7$), strongly mixed in an antibonding fashion with the metal d$_\pi$ orbitals. The LUMO is composed primarily of the lowest unoccupied bridge orbitals, 1π$_g$ (C$_3$) or 2π$_u$ (C$_5$) or 2π$_g$ (C$_7$), strongly mixed in an antibonding fashion with the metal d$_\pi$ orbitals. Due to the filled–filled interaction, the HOMO in the considered dinuclear complexes is significantly higher in energy than the HOMO (of σ symmetry) of the cumulenic bridge (see Fig. 3). Moreover, the nature of the HOMO and LUMO does not suggest for UV transitions a net charge-transfer character, although a partial metal-to-bridge charge-transfer can be considered since the LUMO is more localized on C$_x$. On lengthening the bridging chain from C$_3$ to C$_5$ and C$_7$, several effects are observed as shown in Table 3: (i) the HOMO–LUMO gap decreases, this predicting progressively red-shifted bands in UV–vis spectra of these hypothetical compounds. This is in agreement with the experimental UV–vis spectra for the cumulenic [Cp*Re(NO)(PPh$_3$)(μ-C$_x$)Mn(CO)$_2$(η^2-C$_5$Cl$_5$)] ($x = 3$, 5) species, whose most intense absorptions are red-shifted by 65–80 nm passing from C$_3$ to C$_5$ [22]. (ii) The metal character of the HOMO orbital decreases thus leading to a less marked metal-to-bridge character of the lowest electronic transition. (iii) The HOMO energies of the considered dinuclear complexes decrease (see Table 3) thus predicting that oxidations will become thermodynamically less favorable in the series as the carbon chain increases from C$_3$ to longer odd chains C$_x$. This trend is very similar to that observed and calculated for the even bridging chain (from C$_4$ to C$_{20}$) compounds [5,29], but no experimental data are available for odd bridging chains.

Electron counting

(CO)$_2$CpCr=C=C=C=CrCp(CO)$_2$ 17 e

(CO)$_2$CpMn=C=C=C=MnCp(CO)$_2$ 18 e

(CO)$_2$CpFe—C≡C—C≡CrCp(CO)$_2$ 18 e

Scheme 4.

5.2. Heteronuclear series

The orbital interaction diagram in Fig. 4 shows the most relevant interactions between the metal fragment d$_\pi$ orbitals, separately for iron and chromium, and the π system of the C$_3$ bridging unit. The two main interactions (filled–filled, filled–empty) reported for homonuclear series above can still be distinguished in the heteronuclear series. However, the HOMO orbital is composed primarily of the chromium d$_\delta$ orbital, 17a′ (d$_{z^2}$) while the LUMO is composed mainly of the iron d$_\delta$ orbital, 13a″ (d$_{xz}$). Since these two orbitals have a negligible superposition, we expect a very weak absorption in agreement with the experimental UV–vis spectra of the alkynyl/carbyne [Cp*Re(NO)(PPh$_3$)–C≡C–C≡W(O–t-Bu)$_3$] complex which, at variance of that of the cumulenic [Cp*Re$^+$(NO)(PPh$_3$)=C=C=C=Mn(CO)$_2$(C$_5$H$_c$Cl$_{5-c}$)] species, shows only very weak featureless tails in the visible region [24]. The effects arising from lengthening the bridging chain from C$_3$ to C$_5$, and C$_7$ are reported in Table 4. We observe that: (i)

the HOMO–LUMO gap shows a slight increase on lengthening the chain for these polyynyl/carbyne complexes, probably due to the essentially metal nature of these orbitals which are not connected to the π-frontier orbitals of the C_x chain. (ii) The HOMO energies of the considered dinuclear complexes decrease (see Table 4), suggesting that oxidations become thermodynamically less favorable as the carbon chain increases in these polyynyl/carbyne complexes.

6. Conclusions

In the present investigation we have studied the electronic and geometrical structures of C_x bridged dinuclear complexes. Compounds with an odd C_x bridge are much less common and two different valence structures are possible, i.e. a symmetrical cumulenic structure $L_mM{=}C{=}(C{=}C)_y{=}M'L'_{m'}$ and a unsymmetrical polyynyl/carbyne structure $L_mM{-}(C{\equiv}C)_y{-}C{\equiv}M'L'_{m'}$ with a metal–carbon single bond on one end and a metal–carbon triple bond on the other.

Density functional calculations have been performed on a variety of homonuclear $[\{Cp(CO)_2M\}_2(\mu\text{-}C_x)]$ ($M = Cr, Fe^+, x = 3$; $M = Mn, x = 3, 5, 7$) and heteronuclear $[\{Cp(CO)_2M\}(\mu\text{-}C_x)\{Cp(CO)_2M'\}]$ ($M = Fe^+$, $M' = Mn, x = 3$; $M = Fe, M' = Cr, x = 3, 5, 7$) model complexes close to some available experimental compounds. These calculations showed that the geometrical structure is essentially determined by the nodal pattern of the highest molecular orbitals of d_π–p_π (C_x) character. On the basis of such results we have developed a simple molecular orbital model which allows the prediction of the valence formulation in these complexes.

For the homonuclear series, the HOMO nodal pattern suggests a cumulene-like geometry which is foreseen not to change substantially by adding or subtracting two electrons in complexes based on d^7 and d^5 metal fragments, respectively, evidentiating a special stability of the $L_mMC_xML_m$ complexes based on metal fragments with a d^6 configuration.

For the heteronuclear complexes the nodal pattern of the highest, occupied π-orbitals is modified as a consequence of the different electronegativity of the two metal fragments which breaks the symmetry of these systems. The HOMO nodal pattern suggests, in this case, a partial alkynyl/carbyne geometry, with a triple bond between the least electronegative metal fragment and the adjacent carbon and a single bond between the most electronegative metal fragment and the adjacent carbon. Therefore, the heteronuclear complexes are described by both cumulenic and alkynyl/carbyne resonance forms, the contribution of the latter being the higher the larger is the difference between the electron-attracting properties of the ML_m and $M'L'_{m'}$ metal fragments.

Acknowledgements

Support by the CNR National Project 'Special Materials for Advanced Technologies' is gratefully acknowledged. We thank the CINECA for providing a computer grant.

References

[1] F. Diederich, Y. Rubin, Angew. Chem. Int. Ed. Engl. 31 (1992) 1101.
[2] H. Lang, Angew. Chem. Int. Ed. Engl. 34 (1994) 547.
[3] W. Beck, B. Niemer, M. Wieser, Angew. Chem. Int. Ed. Engl. 32 (1993) 923 (and references therein).
[4] (a) F. Paul, C. Lapinte, Coord. Chem. Rev. 178-180 (1998) 427; (b) M. Akita, Y. Moro-oka, Bull. Chem. Soc. Jpn. 68 (1995) 420; (c) M.I. Bruce, Coord. Chem. Rev. 166 (1997) 91; (d) H. Werner, Chem. Commun. (1997) 903.
[5] (a) R. Dembinski, T. Bartik, B. Bartik, M. Jaeger, J.A. Gladysz, J. Am. Chem. Soc. 122 (2000) 810; (b) W. Mohr, J. Stahl, F. Hampel, J.A. Gladysz, Inorg. Chem. 40 (2001) 3263; (c) B. Bartik, R. Dembinski, T. Bartik, A.M. Arif, J.A. Gladysz, New J. Chem. 21 (1997) 739.
[6] J.R. Heath, Q. Zhang, S.C. O'Brien, R.F. Curl, N.W. Kroto, R.E. Smalley, J. Am. Chem. Soc. 109 (1987) 359.
[7] Q. Fan, G.V. Pfeiffer, Chem. Phys. Lett. 162 (1989) 472.
[8] Y. Zhou, J.W. Seyler, W. Weng, A.M. Arif, J.A. Gladysz, J. Am. Chem. Soc. 115 (1993) 8509.
[9] J.W. Seyler, W. Weng, Y. Zhou, J.-A. Gladysz, Organometallics 12 (1993) 3802.
[10] R. Crescenzi, C. Lo Sterzo, Organometallics 11 (1992) 2301.
[11] T. Rappert, O. Nürnberg, H. Werner, Organometallics 12 (1993) 1359.
[12] M.I. Bruce, R. Hinterding, E.R.T. Tieking, B.W. Skelton, A.H. White, J. Organomet. Chem. 450 (1993) 209.
[13] V.W.W. Yam, C.Y. Lau, K.K. Cheung, Organometallics 15 (1996) 1740.
[14] O. Gevert, J. Wolf, H. Werner, Organometallics 15 (1996) 2806.
[15] E. Viola, C. Lo Sterzo, F. Trezzi, Organometallics 15 (1996) 4352.
[16] W. Weng, T. Bartik, M. Brady, B. Bartik, J.A. Ramsden, A.M. Arif, J.A. Gladysz, J. Am. Chem. Soc. 117 (1995) 11922.
[17] T. Bartik, B. Bartik, M. Brady, R. Dembinski, J.A. Gladysz, Angew. Chem. Int. Ed. Engl. 35 (1996) 414.
[18] N. Le Narvor, C. Lapinte, J. Chem. Soc. Chem. Commun. (1993) 357.
[19] N. Le Narvor, L. Toupet, C. Lapinte, J. Am. Chem. Soc. 117 (1995) 7129.
[20] M. Brady, W. Weng, J.A. Gladysz, J. Chem. Soc. Chem. Commun. (1994) 2655.
[21] F. Coat, C. Lapinte, Organometallics 15 (1996) 477.
[22] T. Bartik, W. Weng, J.A. Ramsden, S. Szafert, S.B. Falloon, A.M. Arif, J.A. Gladysz, J. Am. Chem. Soc. 120 (1998) 11071.
[23] B.E. Woodworth, J.L. Templeton, J. Am. Chem. Soc. 118 (1996) 7418.
[24] R. Dembinski, S. Szafert, P. Haquette, T. Lis, J.A. Gladysz, Organometallics 18 (1999) 5438.
[25] D.R. Neithamer, R.E. LaPointe, R.A. Wheeler, D.S. Richeson, G.D. Van Duyne, P.T. Wolczanski, J. Am. Chem. Soc. 111 (1989) 9056.
[26] K.G. Caulton, R.H. Cayton, R.H. Chisholm, J.C. Huffman, E.B. Lobkovsky, Z. Xue, Organometallics 11 (1992) 321.
[27] J. Heidrich, M. Stelman, M. Appel, W. Beck, J.R. Phillips, W.C. Trogler, Organometallics 9 (1990) 1296.

[28] P. Belanzoni, N. Re, M. Rosi, A. Sgamellotti, C. Floriani, Organometallics 15 (1996) 4264.
[29] P. Belanzoni, N. Re, A. Sgamellotti, C. Floriani, J. Chem. Soc. Dalton Trans. (1998) 1825.
[30] M. Brady, W. Weng, Y. Zhou, J.W. Seyler, A.J. Amoroso, A.M. Arif, M. Böeme, G. Frenking, J.A. Gladysz, J. Am. Chem. Soc. 119 (1997) 775.
[31] M.I. Bruce, P.J. Low, K. Costuas, J.-F. Halet, S.P. Best, G.A. Heath, J. Am. Chem. Soc. 122 (2000) 1949.
[32] H. Jiao, J.A. Gladysz, New J. Chem. 25 (2001) 551.
[33] (a) E.J. Baerends, D.E. Ellis, P. Ros, Chem. Phys. 2 (1973) 41;
(b) E.J. Baerends, P. Ros, Chem. Phys. 2 (1973) 51;
(c) E.J. Baerends, P. Ros, Chem. Phys. 8 (1975) 41;
(d) E.J. Baerends, P. Ros, Int. J. Quantum Chem. S12 (1978) 169.
[34] (a) P.M. Boerrigter, G. te Velde, E.J. Baerends, Int. J. Quantum Chem. 33 (1988) 87;
(b) G. te Velde, E.J. Baerends, J. Comput. Phys. 99 (1992) 84.
[35] T. Ziegler, V. Tschinke, E.J. Baerends, J.G. Snijders, W. Ravenek, J. Phys. Chem. 93 (1989) 3050.
[36] S.H. Vosko, L. Wilk, M. Nusair, Can. J. Phys. 58 (1980) 1200.
[37] A.D. Becke, Phys. Rev. A38 (1988) 2398.
[38] J.P. Perdew, Phys. Rev. B33 (1986) 8822.
[39] (a) J. Chatt, R.C. Fay, R.L. Richards, J. Chem. Soc. A (1971) 2399;
(b) J.M. Treitel, M.T. Flood, R.E. March, H.B. Gray, J. Am. Chem. Soc. 91 (1969) 6512;
(c) D. Sellmann, Angew. Chem. Int. Ed. Engl. 13 (1974) 639.
[40] A.M. Crespi, D.F. Shriver, Organometallics 4 (1985) 1830.
[41] M.D. Johnson, in: G. Wilkinson, F.G.A. Stone, E.W. Abel (Eds.), Comprehensive Organometallic Chemistry, vol. 4, Pergamon Press, Oxford, 1982, p. 331.